Received: 13 March 2024 | Revised: 18 June 2024 | Accepted: 16 July 2024

DOI: 10.1111/jace.20063

Journal of the American Ceramic Society

SPECIAL ISSUE ARTICLE

Molecular dynamics simulations on ferroelectricity of AlN thin films

Binghui Deng | **Jian Shi** | **Yunfeng Shi**

Department of Materials Science and Engineering, Rensselaer Polytechnic Institute, Troy, New York, USA

Correspondence
Binghui Deng and Yunfeng Shi, Department of Materials Science and Engineering, Rensselaer Polytechnic Institute, Troy, NY 12180, USA.
Email: dengb4@rpi.edu and shiy2@rpi.edu

Funding information
National Science Foundation, Grant/Award Numbers: 2015557, 2024972

Abstract

The recent realization of ferroelectricity in scandium- and boron-substituted AlN thin films has spurred tremendous research interests. Here we established a molecular dynamics simulation framework to model the ferroelectricity of AlN thin films. Through reparameterization of Vashishta potential for AlN, the coercive field strength and the AlN polarization were found to be close to experimental values. Furthermore, we examined the effects of film thickness, temperature, in-plane strain on polarization-electric field hysteresis loop, and the thickness-dependent Curie temperature. Lastly, we incorporated electrodes towards atomic-level modeling of ferroelectric device, by considering the induced charge at the interface between electrodes and ferroelectric film. We found that low dielectric contrast significantly lowers the coercive field for switching AlN.

KEYWORDS
aluminum nitride, ferroelectricity/ferroelectric materials, molecular dynamics

1 | INTRODUCTION

Aluminum nitride (AlN) exists primarily in hexagonal polar wurtzite structure with a spontaneous polarization parallel to its *c* axis, along which piezoelectricity and pyroelectricity are manifested.[1,2] As an excellent functional material, AlN has been widely exploited in thin film bulk acoustic wave and micro-electromechanical system devices, such as ultrasonic transducers, acoustic resonators, and energy harvesters, due to a good combination of low dielectric loss, high breakdown strength, high thermal stability, and high mechanical strength.[3–8]

Although typically recognized as being piezoelectric and pyroelectric, AlN was generally not considered as a ferroelectric material due to the lack of experimental demonstration of polarization reversal. This is probably because its dielectric breakdown strength is lower than the coercive field. For instance, Yasuoka et al.,[9] Hayden et al.,[10] and Zhu et al.[11] have explored the ferroelectric switching capability of pure AlN films fabricated by various sputtering methods. Although limited partial polarization switching is indeed present in these films, no clear evidence for solid unambiguous polarization switching could be demonstrated. Interestingly, results from these studies equally obfuscate the authors to conclude or refute the possibility of ferroelectricity in pure AlN thin films due to complexities coming from current leakage and inconsistent thin film quality. It is highly possible to clearly demonstrate polarization reversal by tunning deposition conditions to either reduce in-plane compressive strain or induce in-plane tensile strain to lower the coercive field while not significantly compromising the dielectric breakdown strength.[9,12]

In fact, Lin et al.[13] first demonstrated ferroelectricity in pure AlN ultrathin films (8–10 nm in thickness), employing a strain engineering strategy, by creating a ferroelectric AlN/GaN heterojunction via atomic layer epitaxy. This demonstration of ferroelectricity is believed to stem from

the out-of-plane compressive strain and in-plane tensile strain due to the lattice mismatch at the AlN/GaN interface. However, it is important to emphasize that remnant polarization was measured to be nearly two orders of magnitude lower than the theoretical prediction (~130 $\mu C/cm^2$),[14,15] which calls for further investigation.

Beyond pure AlN thin films, the unambiguous confirmation of ferroelectricity in scandium-substituted $Al_{1-x}Sc_xN$ thin films by Fichtner et al.[15] in 2019, and boron-substituted $Al_{1-x}B_xN$ thin films by Hayden et al.[10] in 2021 has spurred significant research interests. As of now there have been many studies published on the two systems focusing on different aspects of ferroelectricity, such as film composition, temperature, film thickness, deposition condition, and fatigue endurance by electric field cycling, etc.[16,17] Although there have been a number of molecular-level simulations describing the ferroelectric behavior of $BaTiO_3$ and $KNbO_3$,[18–21] there have been no molecular-level simulation studies so far to complement these studies and advance our understanding of the ferroelectric characteristics of AlN-based materials. To fill this gap, we present a molecular dynamics simulation framework to model ferroelectricity in AlN thin films. We reparameterized Vashishta AlN's potential to reproduce the experimental coercive force and remnant polarization for AlN. We further investigated how AlN responds as a ferroelectric material under various electric, thermal, and mechanical stimuli as well as surface charge screening from electrodes. The critical roles of dopants, such as Sc and B as revealed in experiments, are out of scope for this work because it requires the development of new potential that covers these dopant elements, which is the pursuit of our future work.

2 | SIMULATION METHOD

2.1 | Interatomic potential

The force field for pure AlN thin films was based on a well-established interaction potential developed by Vashishta et al.[22] in 2011. Various two-body terms are included to describe steric-size effects, screened Coulombic interactions between point charges as well as charge-induced dipoles, and van der Waals interactions. Vashishta's potential also includes three-body terms accounting for bond-bending. It has been parameterized to reproduce the Wurtize crystal structure, cohesive energy, elastic constants, melting temperature, and dynamic properties of bulk AlN. The two-body part is given by

$$V_{ij}(r) = \frac{H_{ij}}{r^{\eta_{ij}}} + \frac{Z_i Z_j}{r} e^{-r/\lambda} - \frac{D_{ij}}{r^4} e^{-r/\xi} - \frac{W_{ij}}{r^6},$$

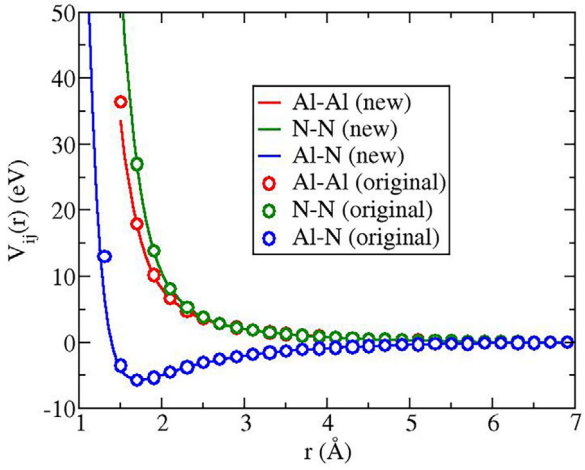

FIGURE 1 Comparison between the species-dependent pairwise term in Vashishta potential as a function of separation distance with the original AlN parameters (circles) and with our new parameters set (lines).

where r is the distance between atom i and atom j, H_{ij} is the strength of the steric repulsion, η_{ij} is the exponent of steric repulsion, Z_i or Z_j is the effective charge, D_{ij} and W_{ij} are the strengths of the charge-dipole attractions and van der Waals attractions, and λ and ξ are the screening lengths for the screened Coulombic interactions between point charges and charge-induced dipoles, respectively.

Interestingly, the potential has an effective charge of $1.0708e$ and $-1.0708e$ for Al and N, respectively, significantly underestimates the AlN remnant polarization and overestimates the coercive force in terms of both experimental measurements and theoretical predictions,[11,14,15] even though it works well for thermal, structural, mechanical, and some dynamical properties of crystalline AlN. To remedy the situation, we increased the charge values to $3e$ and $-3e$ for Al and N and refined the parameters for the two-body interactions, in such a way that the species-dependent pair-wise potential curves almost perfectly overlap the original ones as shown in Figure 1. Although we recognized that the chemical bonds between Al and N are partially covalent as demonstrated by first-principles calculations,[23] the assignment of $3e$ and $-3e$ to Al and N for charge seems to be a convenient yet inevitable solution to study the ferroelectric characteristic of AlN thin films quantitatively. All parameters for three-body interactions remain the same. The potential parameters, along with the original parameters, are listed in Table 1. It should be noted that the parameters in the pair-wise interactions are treated as fitting parameters to reproduce the original overall pair-wise interaction as accurately as possible. As a compromise, those parameters may not represent the originally intended physical contributions.

TABLE 1 The parameter differences between the original Vashishta AlN potential and our re-parameterized Vashishta AlN potential.

		Z_i (e)	λ (Å)	ξ (Å)	r_c (Å)
Original	Al	1.0708	5.0	3.75	7.6
	N	−1.0708			
This study	Al	3	5.0	3.75	7.6
	N	−3			
		η_{ij}	H_{ij} (eV Å$^{\eta}$)	D_{ij} (eV Å^4)	W_{ij} (eV Å^6)
Original	Al–Al	7	507.668	0	0
	Al–N	9	367.055	24.7978	34.583
	N–N	7	1038.163	49.5956	0
This study	Al–Al	1.2891	−113.241	0	−354.087
	Al–N	1.3924	123.566	251.788	−310.545
	N–N	1.2608	−110.447	156.763	−830.807

Note: Only parameters of two-body terms are included as three-body terms are identical.

The AlN system with the new parameter set with 3e and −3e for Al and N behaves quite similarly to the original Vashishta AlN system. For instance, the Wurtzite crystal has a global minimum of 5.856 eV/atom at 10.46 Å^3/atom, compared to 5.764 eV/atom at 10.44 Å^3/atom of the original system. The melting point estimated from a simple heating process is around 3200 K, which is slightly higher than ~3000 K using the original Vashishta potential.

2.2 | Simulation setup

The compensation of polarization-induced surface charges is critical for the ferroelectric stability of nanoscale thin films.[24] Insufficient screening of the surface charges will result in a depolarization field to oppose bulk polarization, thereby compromising ferroelectricity.[25] In typical ferroelectric devices, the surface charge is screened by sandwiching the film using two metallic electrodes. To account for the effect, we set up the simulations by taking advantage of a method developed by Nguygen et al.[26] in which the induced charges at the film/electrode interface is modeled by the boundary element method at the continuum level with given dielectric contrast. The induced charges at the boundary elements are determined by solving Poisson's equation using the generalized minimum residual solver, as detailed in the studies.[27,28] As shown in Figure 2, the interface is discretized into vertices arranged in two-dimensional hexagonal lattices (each representing a boundary element) with a lattice constant of 1.56 Å, which are treated as if they were regular atoms or particles with unit molar mass and dielectric properties assigned. Specifically, we set the dielectric contrast with AlN being five based on measurement detailed in the Supporting Information Material, and that of electrode $\kappa_{electrode}$ being in the range of 5 to 15 to study the surface charge effect on ferroelectricity. It is worth mentioning that the surface charge effect can be easily turned off when there is no dielectric contrast ($\kappa_{electrode} = \kappa_{AlN} = 5$), in which case the intrinsic ferroelectric characteristics of AlN thin film are probed (Sections 3.1–3.3).

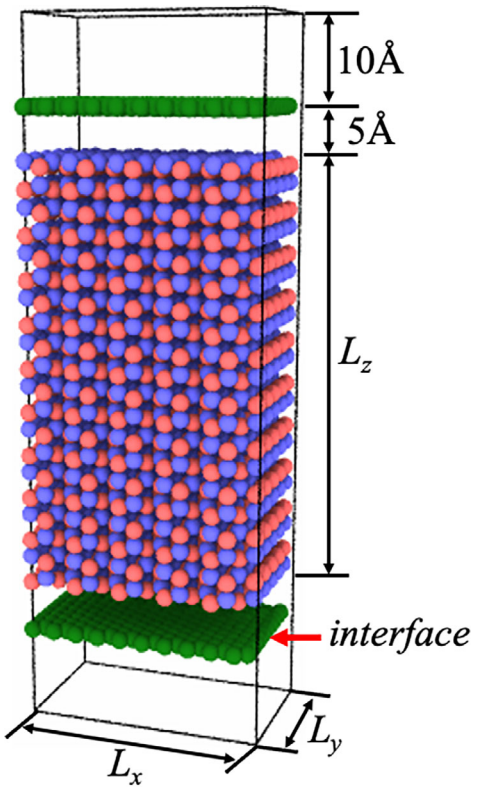

FIGURE 2 Simulation setup for AlN thin film subjected to electric field in the z-direction. Al and N atoms are colored blue and red, respectively. The film thickness L_z varies from 1.5 to 15 nm, with the other two dimensions fixed at 2.72 nm (L_x) and 1.57 nm (L_y), respectively. The AlN/electrode interface is discretized into vertices (green) that are treated as regular particles with a specified mean dielectric constant (($\kappa_{electrode} + \kappa_{AlN}$)/2).

The AlN thin film was constructed with Wurtzite crystal structure (a = 3.112 Å, c = 4.982 Å) with different thickness L_z (along [0001] direction) ranging from 1.5 to 15 nm, with the other two dimensions fixed at 2.72 nm (L_x, along [1$\bar{1}$00] direction) and 1.57 nm (L_y, along [11$\bar{2}$0] direction), respectively. The film/electrode interface was initially positioned 5 Å away from the film surface. For simplicity, the Coulombic interaction among the boundary elements, and between boundary elements and AlN film has a cutoff of 15 Å, without considering the long-range effects. In addition, a Lennard–Jones pair-wise interaction (repulsive only) between AlN and the boundary elements was included to prevent the implosion of ions with their induced charges, with ε of 1.0 eV, σ of 4.45 Å, and cutoff of 5 Å. The boundary elements representing the two interfaces can move as rigid bodies along the z-direction to maintain zero stress. The simulation box was padded with an extra 10 Å on both sides along the z-direction to ensure the thin film nature of the simulation system. Periodic boundary conditions, instead, were applied in the other two dimensions.

All the simulations were run using LAMMPS[29] with a timestep of 1 fs. Temperature and pressure were well controlled via Nose[30] and Hoover[31] thermostat and barostat, respectively. Electric field strength was ramped up with a step of 0.0667 MV/cm every 0.3 ps before it was ramped down to reverse the field direction at the same rate. The total simulation time for a complete P–E hysteresis loop is 576 ps. The OVITO[32] software was used to visualize the atomic structure and simulation process.

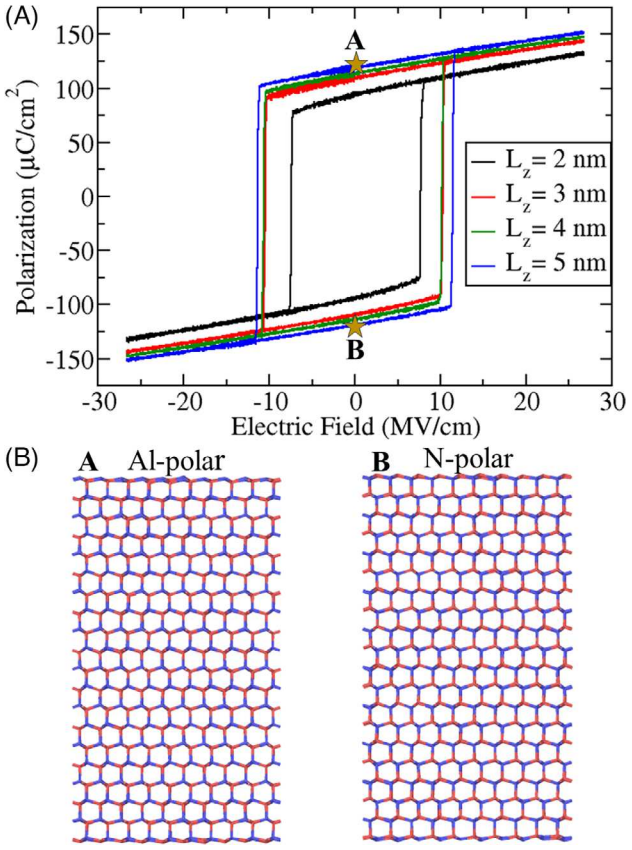

FIGURE 3 (A) The polarization-electric field (P–E) loop for AlN films with different thickness ranging from 2 to 5 nm at 300 K. (B) The representative structure change before (Al-polar) and after (N-polar) polarization reversal for the 5 nm thick film. Note that the structure is shown with bond instead of atoms for better visualization.

3 | RESULTS AND DISCUSSION

3.1 | Thickness-dependent ferroelectric response

Understanding the thickness-dependent ferroelectric response of thin film is the key to miniaturize ferroelectric devices and reduce power consumption because it typically loses polarization stability once the thickness approaches ~100 nm, with different thickness limits depending on specific film chemistry and processing conditions. Figure 3A shows the polarization–electric field (P–E) loop for AlN films with different thicknesses ranging from 2 to 5 nm at 300 K. All films exhibit a nearly ideal boxlike ferroelectric loop with clean polarization reversal at corresponding coercive electric field. The remnant polarization for the 5 nm sample is around 130 μC/cm^2, which agrees closely with theoretical calculation and experimental extrapolations. Additionally, both the P_r and E_c monotonically decrease when the film thickness is scaled down, with the 2 nm film being considerably lower than the others, which suggests that 2 nm is the thickness limit for AlN films to remain solid ferroelectric stability because the P–E loop for a 1.5 nm thick film starts to fail in maintaining the box-like hysteresis loop.

Figure 3B shows the structure change before and after polarization reversal for the 5 nm thick film. The ferroelectric switching is clearly manifested with the Al-polar state switching to the N-polar state. It is worth mentioning that E_c is over 10 MV/cm even for the 2 nm thick film, which might have exceeded the dielectric breakdown limit according to experimental extrapolations, and, unfortunately, we cannot extract the dielectric breakdown limit using this simulation setup. However, we argue that the model is still very valuable since it offers a venue for us to probe many fundamentals of ferroelectric characteristics for AlN thin films as demonstrated in the following sections.

Thermal stability is another important aspect of ferroelectric materials. The spontaneous polarization will vanish when a critical temperature T_c is reached, at which the polarization-associated polar structure gets destroyed.

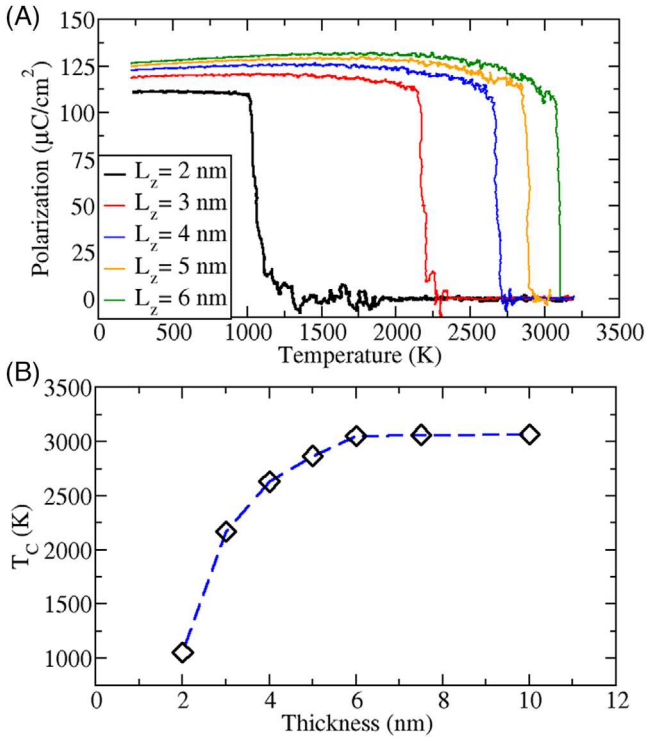

FIGURE 4 (A) The polarization evolution as a function of temperature for AlN films with different thicknesses, from which the transition temperature T_c can be clearly identified. (B) The corresponding thickness dependence of T_c for AlN thin films.

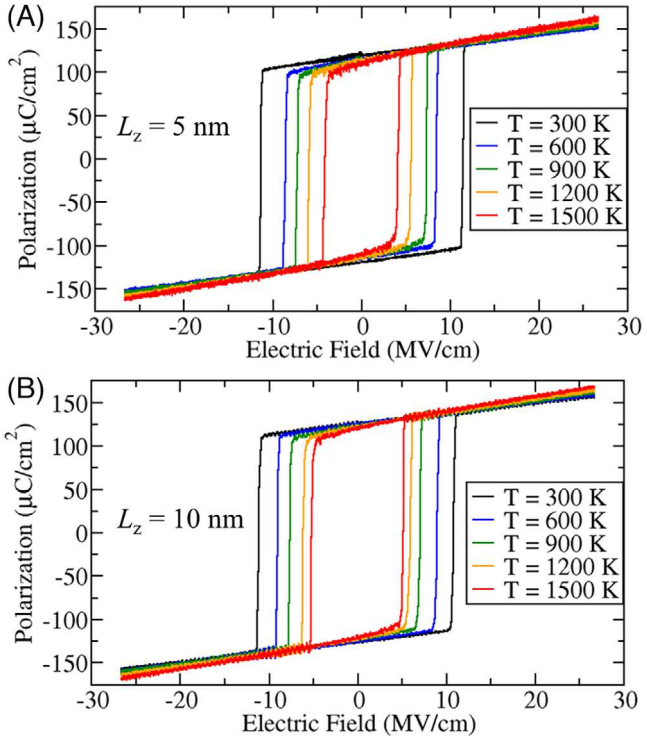

FIGURE 5 The temperature dependence of ferroelectric switching for AlN thin films with thickness of 5 nm (A) and 10 nm (B), respectively.

The film thickness dependence of T_c has been reported in many studies for various systems, which manifests as a sharp drop of T_c as the film thickness approaches its corresponding thickness limit that retains polarization. Figure 4A shows the polarization evolution as a function of temperature for AlN films with different thicknesses, from which the T_c of each film can be clearly identified. Accordingly, Figure 4B shows the thickness dependence of T_c for AlN thin film. Similar to the trend observed for single crystalline $BaTiO_3$ nanowires,[25] T_c drops rapidly when the thickness approaches 2 nm, while saturates when the thickness is over 6 nm. The working mechanism that underlies the thickness dependence of T_c could be well understood based on Landau–Devonshire theory and associated works.[33–35] One primary driver is the reduced surface polarization due to depolarization fields, particularly in the scenario wherein no effective surface charge screening mechanisms are present.

3.2 | Temperature-dependent ferroelectric response

Figure 5A, B shows the temperature dependence of ferroelectric switching for AlN thin films with thickness of 5 and 10 nm, respectively. The temperature varied from 300 to 1500 K, far below the corresponding T_c as shown in Figure 4B. For both systems, the *P*–*E* loop trends with temperature in a nearly identical way, with both P_r and E_c decreasing with increasing temperature. Interestingly, the reduction for E_c is more pronounced than P_r, which agrees closely with experimental results on AlN, $Al_{1-x}Sc_xN$, and $Al_{1-x}B_xN$ thin films reported by Zhu et al.[11]

3.3 | In-plane strain-dependent ferroelectric response

Besides temperature, strain is another useful engineering approach to control ferroelectricity. For instance, Yashuoka et al.[36] deposited a 145 nm thick $Al_{0.8}Sc_{0.2}N$ film on various substrates with different thermal expansion coefficients (CTE), including fused silica, Si, Al_2O_3, and MgO, to generate different levels of strains in the films driven by the CTE mismatch. Specifically, films deposited on fused silica and Si substrates underwent in-plane compressive stress, while films deposited at Al_2O_3 and MgO substrates underwent in-plane tensile stress. It was found that E_c would get reduced considerably when more tensile strain was installed in the film.

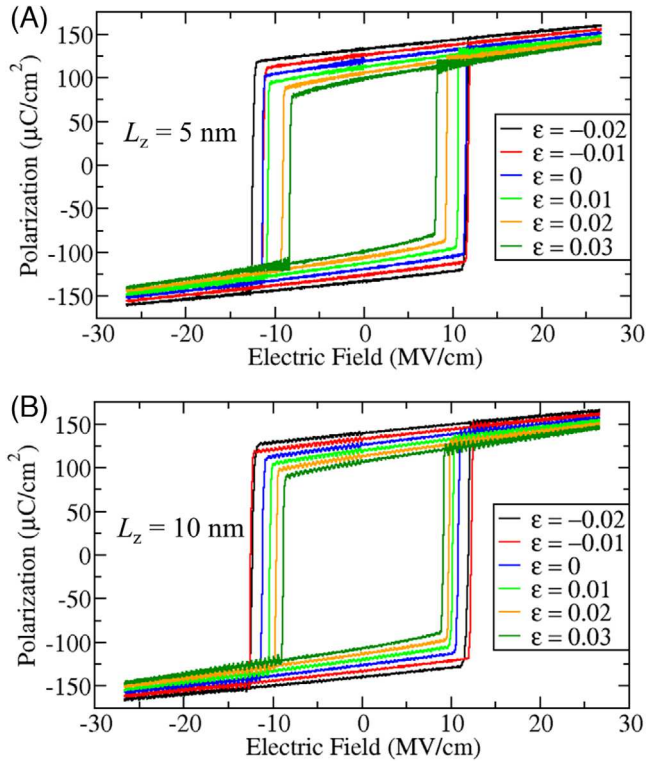

FIGURE 6 The in-plane strain dependence of ferroelectric switching for AlN thin films with thickness of 5 nm (A) and 10 nm (B), respectively.

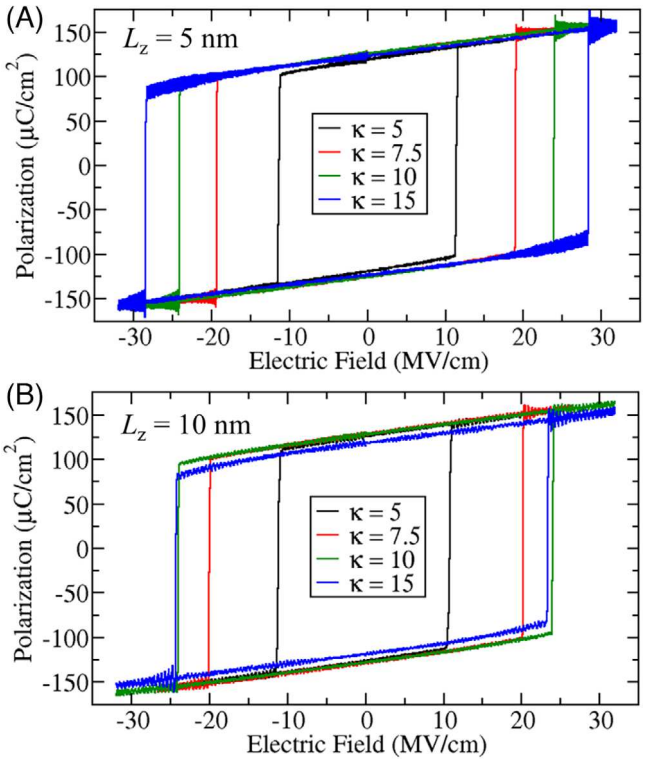

FIGURE 7 The *P–E* loop dependence on dielectric contrast for AlN thin films with thickness of 5 nm (A) and 10 nm (B), respectively.

In alignment with experimental studies, we installed different amounts of bi-axial in-plane strains, from −0.02 to 0.03, before applying an electric field for AlN thin films. Figure 6A, B shows the strain dependence of ferroelectric switching for films with thickness of 5 and 10 nm, respectively. Similar to the temperature dependence, the *P–E* loop for both systems trends with strain in a nearly identical way, with E_c getting reduced when the strain moves from compressive to tensile. The reduction becomes more noticeable in a tensile strain regime.

3.4 | Effect of surface charge screening on ferroelectric response

Nanoscale ferroelectric films are very sensitive to polarization-induced surface charges, with insufficient screening compromising ferroelectric stability. We explore this effect by generating dielectric contrast using $\kappa_{\text{electrode}}$ and κ_{AlN} as mentioned in Section 2.2. In other words, the higher the $\kappa_{\text{electrode}}$ is, the more effective it is to screen surface charges. Similarly, Figure 7A, B shows the *P–E* loop dependence on dielectric contrast for films with thickness of 5 and 10 nm, respectively. The dielectric constant $\kappa_{\text{electrode}}$ varies from 5 to 15, while κ_{AlN} keeps constant at 5. Indeed, the dielectric contrast has a dramatic influence on the ferroelectric characteristics of AlN films, with E_c nearly doubles for the highest dielectric contrast case. Interestingly, the effect seems to decay more quickly for the thicker 10 nm film because there is a very marginal difference between $\kappa_{\text{electrode}}$ of 10 and 15, which suggests that any approaches to screening surface charge will considerably improve the ferroelectric stability of ultrathin films.

4 | CONCLUSION

The recent unambiguous realization of ferroelectricity in scandium- and boron-substituted AlN thin films has intrigued scientists worldwide. Even though there have been a considerable number of experimental studies focusing on different aspects of ferroelectricity, no MD simulation studies have come up so far to develop a complementary understanding at the atomic level. In this work, we are dedicated to offering a molecular dynamics simulation framework to model ferroelectricity for AlN thin films, with the following primary contributions: (1) The original Vashishta atomic interaction for AlN was successfully re-parameterized so that the magnitude of polarization and coercive field strength agree reasonably well to experimental observations. (2) The model enables observation of

ferroelectric switching with a nearly ideal boxlike *P–E* hysteresis loop, and the effects of film thickness, temperature, and in-plane strain on ferroelectric characteristics agree extremely well with experimental observations. (3) The effect of polarization-induced surface charge was also successfully incorporated, which opens the door to not only study the intrinsic ferroelectric characteristics of AlN but also the role of surface charge screening by electrode at the device level.

ACKNOWLEDGEMENTS

The authors thank the support from the National Science Foundation of the United States under Grants 2024972 and 2015557, and the Center for Computational Innovations at Rensselaer Polytechnic Institute.

ORCID

Binghui Deng https://orcid.org/0000-0002-0460-4990
Jian Shi https://orcid.org/0000-0003-2115-2225
Yunfeng Shi https://orcid.org/0000-0003-1700-6049

REFERENCES

1. Fei C, Liu X, Zhu B, Li D, Yang X, Yang Y, et al. AlN piezoelectric thin films for energy harvesting and acoustic devices. Nano Energy. 2018;51:146–61.
2. Stan GE, Botea M, Boni GA, Pintilie I, Pintilie L. Electric and pyroelectric properties of AlN thin films deposited by reactive magnetron sputtering on Si substrate. Appl Surf Sci. 2015;353:1195–202.
3. Piazza G, Stephanou PJ, Pisano AP. Piezoelectric aluminum nitride vibrating contour-mode MEMS resonators. J Microelectromechanical Syst. 2006;15:1406–18.
4. Yarar E, Hrkac V, Zamponi C, Piorra A, Kienle L, Quandt E. Low temperature aluminum nitride thin films for sensory applications. AIP Adv. 2016;6:075115.
5. Dubois M-A, Muralt P. Properties of aluminum nitride thin films for piezoelectric transducers and microwave filter applications. Appl Phys Lett. 1999;74:3032–34.
6. Marauska S, Hrkac V, Dankwort T, Jahns R, Quenzer HJ, Knöchel R, et al. Sputtered thin film piezoelectric aluminum nitride as a functional MEMS material. Microsyst Technol. 2012;18:787–95.
7. Elfrink R, Kamel TM, Goedbloed M, Matova S, Hohlfeld D, van Andel Y, et al. Vibration energy harvesting with aluminum nitride-based piezoelectric devices. J Micromech Microeng. 2009;19:094005.
8. Yoshino Y. Piezoelectric thin films and their applications for electronics. J Appl Phys. 2009;105:061623.
9. Yasuoka S, Shimizu T, Tateyama A, Uehara M, Yamada H, Akiyama M, et al. Effects of deposition conditions on the ferroelectric properties of (Al1−xScx)N thin films. J Appl Phys. 2020;128:114103.
10. Hayden J, Hossain MD, Xiong Y, Ferri K, Zhu W, Imperatore MV, et al. Ferroelectricity in boron-substituted aluminum nitride thin films. Phys Rev Mater. 2021;5:044412.
11. Zhu W, Hayden J, He F, Yang J-I, Tipsawat P, Hossain MD, et al. Strongly temperature dependent ferroelectric switching in AlN, Al1-xScxN, and Al1-xBxN thin films. Appl Phys Lett. 2021;119:062901.
12. Zhang S, Holec D, Fu WY, Humphreys CJ, Moram MA. Tunable optoelectronic and ferroelectric properties in Sc-based III-nitrides. J Appl Phys. 2013;114:133510.
13. Lin B-T, Lee W-H, Shieh J, Chen M-J. Ferroelectric AlN ultrathin films prepared by atomic layer epitaxy. in:Proc. SPIE 10968, Behavior and Mechanics of Multifunctional Materials XIII. 2019. 1096816. https://doi.org/10.1117/12.2522119
14. Dreyer CE, Janotti A, Van De Walle CG, Vanderbilt D. Correct implementation of polarization constants in wurtzite materials and impact on III-nitrides. Phys Rev X. 2016;6:021038.
15. Fichtner S, Wolff N, Lofink F, Kienle L, Wagner B. AlScN: A III-V semiconductor based ferroelectric. J Appl Phys. 2019;125:114103.
16. Deng B, Zhang Y, Shi Y. Examining the ferroelectric characteristics of aluminum nitride-based thin films. J Am Ceram Soc. 2024;107:1571–81.
17. Wang P, Wang D, Mondal S, Hu M, Liu J, Mi Z. Dawn of nitride ferroelectric semiconductors: from materials to devices. Semicond Sci Technol. 2023;38:043002.
18. Zhang Y, Hong J, Liu B, Fang D. Strain effect on ferroelectric behaviors of BaTiO3 nanowires: a molecular dynamics study. Nanotechnology. 2009;21:015701.
19. Sang Y, Liu B, Fang D. The size and strain effects on the electric-field-induced domain evolution and hysteresis loop in ferroelectric BaTiO3 nanofilms. Comput Mater Sci. 2008;44:404–10.
20. Akbarian D, Yilmaz DE, Cao Y, Ganesh P, Dabo I, Munro J, et al. Understanding the influence of defects and surface chemistry on ferroelectric switching: a ReaxFF investigation of $BaTiO_3$. Phys Chem Chem Phys. 2019;21:18240–49.
21. Khadka R, Keblinski P. Molecular dynamics study of domain switching dynamics in $KNbO_3$ and $BaTiO_3$. J Mater Sci. 2022;57:12929–46.
22. Vashishta P, Kalia RK, Nakano A, Rino JP. Interaction potential for aluminum nitride: a molecular dynamics study of mechanical and thermal properties of crystalline and amorphous aluminum nitride. J Appl Phys. 2011;109:033514.
23. Karch K, Bechstedt F. Ab initio lattice dynamics of BN and AlN: covalent versus ionic forces. Phys Rev B. 1997;56:7404–15.
24. Shaw TM, Trolier-McKinstry S, McIntyre PC. The properties of ferroelectric films at small dimensions. Annu Rev Mater Sci. 2000;30:263–98.
25. Spanier JE, Kolpak AM, Urban JJ, Grinberg I, Ouyang L, Yun WS, et al. Ferroelectric phase transition in individual single-crystalline BaTiO3 nanowires. Nano Lett. 2006;6:735–39.
26. Nguyen TD, Li H, Bagchi D, Solis FJ, Olvera de la Cruz M. Incorporating surface polarization effects into large-scale coarse-grained molecular dynamics simulation. Comput Phys Commun. 2019;241:80–91.
27. Barros K, Luijten E. Dielectric effects in the self-assembly of binary colloidal aggregates. Phys Rev Lett. 2014;113:017801.
28. Barros K, Sinkovits D, Luijten E. Efficient and accurate simulation of dynamic dielectric objects. J Chem Phys. 2014;140:064903.
29. Plimpton S. Fast parallel algorithms for short-range molecular dynamics. J Comput Phys. 1995;117:1–19.

30. Nosé S. A unified formulation of the constant temperature molecular dynamics methods. J Chem Phys. 1984;81:511–19.
31. Hoover WG. Canonical dynamics: equilibrium phase-space distributions. Phys Rev A. 1985;31:1695–97.
32. Stukowski A. Visualization and analysis of atomistic simulation data with OVITO–the open visualization tool. Model Simul Mater Sci Eng. 2009;18:015012.
33. Wang XS, Wang CL, Zhong WL, Xue XY. Temperature dependence of the critical size of ferroelectric thin films. Ferroelectrics. 2003;282:49–56.
34. Tilley DR, Žekš B. Landau theory of phase transitions in thick films. Solid State Commun. 1984;49:823–28.
35. Wang YG, Zhong WL, Zhang PL. Surface and size effects on ferroelectric films with domain structures. Phys Rev B. 1995;51:5311–14.
36. Yasuoka S, Mizutani R, Ota R, Shiraishi T, Shimizu T, Uehara M, et al. Tunable ferroelectric properties in wurtzite (Al0.8Sc0.2)N via crystal anisotropy. ACS Appl Electron Mater. 2022;4:5165–70.

SUPPORTING INFORMATION

Additional supporting information can be found online in the Supporting Information section at the end of this article.

How to cite this article: Deng B, Shi J, Shi Y. Molecular dynamics simulations on ferroelectricity of AlN thin films. J Am Ceram Soc. 2024;107:7850–57. https://doi.org/10.1111/jace.20063